mater.scichina.com link.springer.com
Published online 25 March 2024 | https://doi.org/10.1007/s40843-023-2846-5
Sci China Mater 2024, 67(4): 1202–1208

SPECIAL TOPIC: Computation-assisted Materials Screening and Design

Prediction of intrinsic two-dimensional topological insulators in Y_3-/X_3Y_4-tetrahydroxybenzene metal–organic networks

Yiyang Yin[1], Yixuan Gao[1], Lizhi Zhang[2], Yu-Yang Zhang[1*] and Shixuan Du[1]

ABSTRACT **Using high-throughput density functional theory calculations, we investigate 232 honeycomb–Kagome metal–organic networks formed by two types of metal clusters and tetrahydroxybenzene (THB) molecules. Among the metal–organic frameworks (MOFs) formed with THB molecules and tri-metallic nanoclusters (referred to as Y_3-THB), we find that seven structures are intrinsically topologically nontrivial. By introducing post-transition metal atoms (Tl, Pb, and Bi), nine intrinsic organic topological insulator candidates with considerably larger spin–orbit coupling gaps are discovered among the structure family X_3Y_4-THB. Typically, the α-Pb_3Zn_4-THB structure has a nontrivial gap of 97.5 meV, almost four times larger than its flat bandwidth (22.5 meV), which can be an ideal platform for realizing the fractional quantum Hall effect. This study provides a new avenue for designing two-dimensional (2D) topological MOFs with large topological band gaps.**

Keywords: high-throughput, two-dimensional, topological insulator, metallic cluster, metal–organic framework, flat band

INTRODUCTION

The presence of unique symmetry-protected edge states within bulk band gaps has led to considerable interest in two-dimensional (2D) topological insulators (TIs), with potential applications in quantum computation and spintronics [1–10]. Thus far, most researches in this field have focused on inorganic materials with confirmed experimental existence. However, organic TIs (OTIs), particularly metal–organic framework (MOF) structures, have garnered considerable attention [11–13] due to the vast array of organic compounds and their versatile combinations. Over the past decade, numerous OTIs have been predicted and explored theoretically, featuring diverse configurations such as honeycomb lattice [14–17], Kagome lattice [18–21], and Lieb lattice [22]. Despite the large number of theoretically predicted systems, only a few of them, such as Cu/Au-dicyanoanthracene (DCA) [23–26] and nickel bis(dithiolene) [27,28], have been synthesized experimentally. Thus, the realization of the quantum spin/anomalous Hall effect (QSHE/QAHE) in 2D organic systems remains challenging in experimental and theoretical research.

The realization of 2D-OTIs faces two challenging aspects within an academic context. First, most 2D organic structures inherently exhibit semiconductive behavior. Second, because of their elemental composition, the spin–orbit coupling (SOC) effect in 2D MOF structures remains notably small. The prevailing research concentrates on MOF structures comprising single metal atoms and organic ligands, with efforts aimed at adjusting the Fermi level and SOC strength through metal element modifications. Nevertheless, this approach may have implications for the coordination properties of the structure, potentially compromising overall system stability. Hence, achieving 2D-OTIs demands careful consideration and thoughtful design to surmount these complexities effectively. Interestingly, a 2D MOF containing Cu trimers has been confirmed to exist [29]. Moreover, a type of MOF with heterometallic clusters comprising Bi and Cu can stabilize with organic linkages [30]. These findings inspire us to believe that inducing multinuclear metal clusters into the 2D OTIs is a practical design strategy. By switching some of the metal atoms in the clusters, electron doping that tunes the position of the Fermi level can be realized without influencing the coordination characteristics of the structure. Large SOC gaps can be realized by inducing post-transition metal atoms (Tl, Pb, and Bi) into the metal clusters. This intriguing experimental research prompted us to search for MOFs based on multinuclear metal clusters. Such MOF structures can potentially overcome the limitations of single metal atom-based MOFs, enabling more precise control over the Fermi level and SOC strength without compromising the coordination properties of the structure.

In this study, we comprehensively explore 2D-OTIs formed by combining metal clusters and tetrahydroxybenzene (THB) molecules, employing high-throughput density functional theory (DFT) calculations. By systematically investigating 232 MOF structures involving diverse transition metal elements and configurations, we identify 16 intrinsic TIs. Notably, this set includes ferromagnetic (FM) and nonmagnetic (NM) materials. Among these 16 OTIs, the α-Pb_3Zn_4-THB structure is particularly remarkable because it possesses topological flat bands (TFBs) and a considerably large SOC gap of 97.5 meV. Our findings suggest that incorporating metal clusters represents a novel and promising avenue for the design of 2D OTIs. Notably, the introduction of heavy metal atoms into these clusters proves

[1] University of Chinese Academy of Sciences and Institute of Physics, Chinese Academy of Sciences, Beijing 100191, China
[2] National Center for Nanoscience and Technology, Beijing 100191, China
* Corresponding author (email: zhangyuyang@ucas.ac.cn)

to be an effective strategy for enhancing SOC gaps.

COMPUTATIONAL DETAILS

All the calculations performed in the high-throughput screening process are based on first-principles DFT calculations using the Vienna *ab initio* simulation package [31] with the projector augmented wave method; the Perdew–Burke–Ernzerhof generalized gradient approximation [32] is adopted for the exchange–correlation functional. The energy cutoff of the plane-wave basis sets is 520 eV, and a 5 × 5 × 1 *k*-mesh grid is used for the self-consistent total energy calculation. In all the calculations, a 15-Å vacuum layer is used, and all atoms are fully relaxed until the residual force on each atom is less than 0.01 eV $Å^{-1}$.

RESULTS AND DISCUSSION

The structure schematics of the two MOF families investigated in this work, Y_3-THB and X_3Y_4-THB, are shown in Fig. 1. Both structures contain a Kagome sublattice formed by THB molecules (marked by the blue dashed line) and a honeycomb sublattice formed by metal clusters. Two different configurations are considered for each family: an α configuration (Fig. 1a, c), in which each transition metal atom bonds with one THB molecule, and a β configuration (Fig. 1b, d), in which each transition metal atom bonds with two THB molecules. The unit cell of these MOFs (marked by a black rhombus) involves two metal clusters and three THB molecules. Each THB molecule contains four hydroxy groups on one benzene ring that are dehydrogenated to bond with the metal atoms. The α and β configurations are combined honeycomb and Kagome lattices with *D6h* symmetry; thus, they should have typical Kagome or honeycomb bands that are topologically nontrivial near the Fermi level. By altering transition metal atom Y, we aim to tune the position of the Fermi level into the topological nontrivial gaps of the Kagome or honeycomb bands to obtain intrinsic TIs.

To date, most predicted 2D-OTIs have narrow SOC gaps, making the quantum Hall effect difficult to realize in these systems. To address this challenge, we propose a novel approach involving the introduction of post-transition metals such as Tl, Pb, and Bi into the clusters. These heavy elements are known for their high SOC strength. This concept leads us to investigate a new class of structures denoted as X_3Y_4-THB, as depicted in Fig. 1c, d, where "X" represents the post-transition metal atoms. Additionally, we incorporate an additional transition metal atom "Y" at the center of the cluster, thereby enhancing the overall stability of the structure. In particular, such clusters have been verified to be feasible in the context of 2D-MOF systems [30], making them a viable and promising consideration for our study. By incorporating these innovative X_3Y_4-THB structures, we aim to explore the potential for enhanced topological properties and open up exciting avenues for realizing 2D TIs with outstanding performance.

Fig. 2 shows the flow of the high-throughput calculation performed in this work. By altering transition metal atom Y and post-transition metal atom X (Tl, Pb, and Bi) in the structures demonstrated above, we obtain 232 initial MOF structures for study. Then, to evaluate the stability of these structures, we screen them in terms of formation energy E_F, which is defined as follows:

$$E_F = E_{MOF} - nE_{THB} - \Sigma E_{metal}, \quad (1)$$

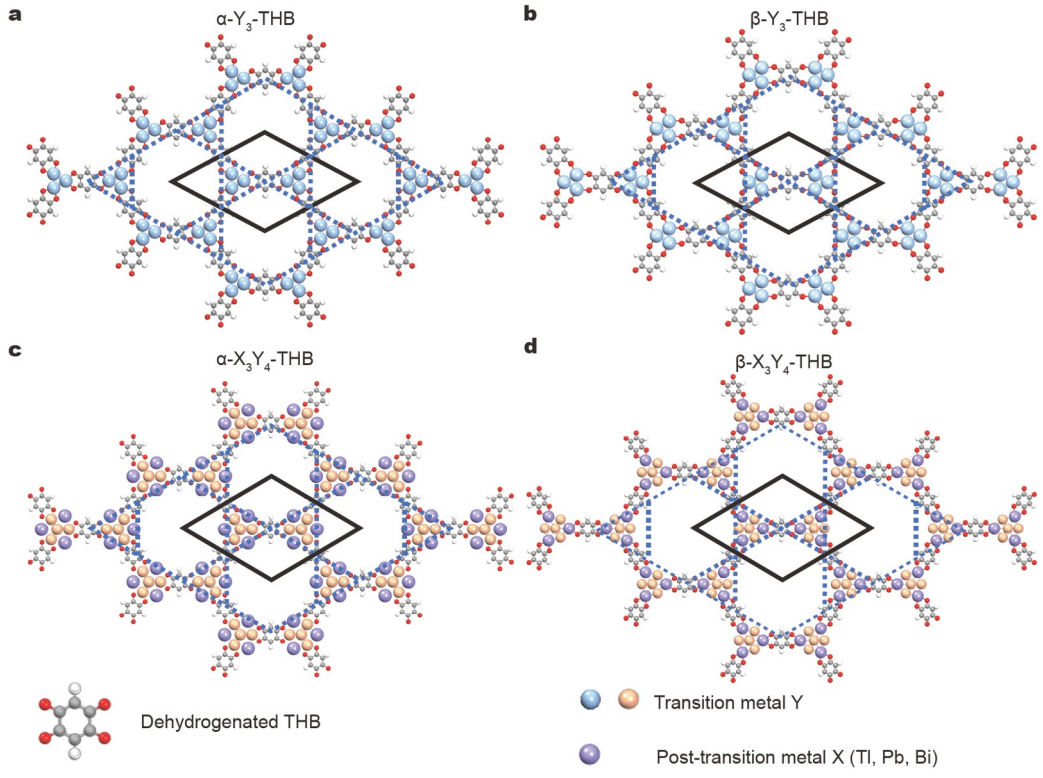

Figure 1 Schematic atomic structures of (a, b) Y_3-THB and (c, d) X_3Y_4-THB. Two configurations of each, named α and β, are demonstrated on the left (a, c) and right (b, d). The inset on the bottom left shows the dehydrogenated THB molecular unit. The blue dashed line and black solid line outline the Kagome sublattice formed by THB molecules and the unit cell, respectively.

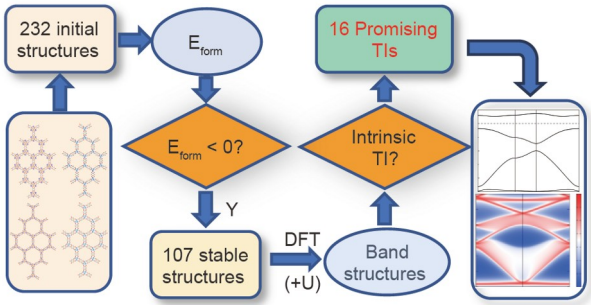

Figure 2 Schematic of the high-throughput workflow conducted in this work.

where E_{THB} refers to the energy of a THB molecule, n is the number of THB molecules in a unit cell (which is three in this case), and E_{metal} is the energy of one metal atom calculated by averaging the energy of the corresponding elemental metal substances by the number of atoms. The full data of the calculated E_F values can be found in Tables S1 and S2. All structures with $E_F > 0$ are considered thermodynamically unstable and are excluded from the candidate list in the following calculations.

After removing thermodynamically unstable structures, we were left with 107 viable candidates for further investigation. Subsequently, we performed DFT calculations on these structures to derive their respective band structures. Because on-site Coulomb interactions are essential in many MOF systems with transition metal elements [33], we include the DFT + U method by Dudarev *et al.* [34] in our calculations. Because of the semiempirical nature of the Hubbard U model, candidates that are only intrinsic TIs under certain U values are deemed "uncertain TI candidates" and excluded from the list of TI candidates. Ultimately, 16 TIs are identified, with topological properties robust to U. Table 1 lists their compositions, formation energies, calculated magnetic ground states (MGS), and SOC band gaps. Their electronic band structures are presented in Fig. S1.

According to the candidate list, most candidates resilient to U interactions are composed of transition metal elements with half-filled or full-filled d orbitals, typically elements from groups IB and IIB. Particularly, within the screening process, we have identified four of the 16 TIs that exhibit TFBs positioned precisely at the Fermi level. This exciting finding holds great promise for the potential realization of the fractional quantum Hall effect (FQHE). As postulated by Tang *et al.* [35], the presence of TFB systems with a substantially larger SOC gap (Δ) than the flat bandwidth (W) strongly favors the emergence of fractional quantum Hall states, particularly when the flat band is partially filled.

Among the six TI candidates featuring TFBs, as listed in Table 1, α-Zn_3-THB, α-Cd_3-THB, and α-Hg_3-THB exhibit remarkably similar band structures and topological properties. Consequently, we designate α-Zn_3-THB as the representative material for comparison with α-Pb_3Zn_4-THB, the most promising candidate possessing a flat band. The notably different SOC gaps of these two structures indicate the effectiveness of our strategic approach to introducing heavy elements into the system.

Fig. 3 demonstrates the electronic structures and topological properties of α-Zn_3-THB. According to our calculations, α-Zn_3-THB exhibits an FM ground state with a magnetic moment of 2 μB per unit cell and lying 11 meV below the antiferromagnetic state. For an isolated dehydrogenated THB molecule, four dehydrogenated hydroxy groups and delocalized p electrons of the benzene ring present a total magnetic moment of 2 μB, as presented in Fig. S2. From Fig. 3a, we clearly find that the magnetic moment is mainly located on oxygen atoms and delocalized p electrons of THB molecules, and the magnetic moment of α-Zn_3-THB should originate from the dehydrogenated THB molecules' intrinsic spin polarization. After forming the α-Zn_3-THB network, the bonds between Zn atoms and the dehydrogenated hydroxy groups partly suppress the spin polarization of the dehydrogenated molecules, leading to a magnetic moment of 2 μB per unit cell.

Fig. 3a demonstrates the band structure and projected density of states (DOS) of α-Zn_3-THB. Notably, the bands around the Fermi level exhibit distinctive and characteristic Kagome bands comprising a flat band and two Dirac bands. Importantly, the Fermi level is precisely located between the flat band and the Dirac bands, proving that α-Zn_3-THB qualifies as an intrinsic flat band TI. Analyzing the PDOS reveals that the Kagome bands predominantly arise from the p_z electrons of the THB molecules, while the Zn metal clusters contribute minimally to these bands. This observation aligns with the structural characteristics of α-Zn_3-THB, where the Kagome sublattice is formed by the THB molecules. Fig. 3b shows the band structure considering SOC. SOC opens a 0.2 meV nontrivial SOC gap at the Γ point near the Fermi level. Fig. 3c presents a tight banding model fitting of the SOC band based on maximum localized Wannier functions (MLWFs), which is implemented in the package Wannier90 [36]. Further calculation shows that the Chern number is 1,

Table 1 Properties of 16 2D-OTIs: summarized results of the TI candidates found in the high-throughput screening process[a]

Structure	E_F (eV uc^{-1})	MGS	E_g^{SOC} (meV)
α-Zn_3-THB*	−14.21	FM	0.2
α-Nb_3-THB	−2.60	FM	12.7
α-Cd_3-THB*	−11.78	FM	0.5
α-Hg_3-THB*	−7.61	FM	0.5
α-Tl_3Cu_4-THB	−4.56	FM	0.8
α-Tl_3Zn_4-THB	−12.47	FM	0.6
α-Pb_3Cu_4-THB	−4.00	NM	2.2
α-Pb_3Zn_4-THB*	−6.84	NM	97.5
α-Pb_3Pd_4-THB	−2.41	NM	1.9
α-Pb_3Pt_4-THB	−3.22	NM	25.1
β-Zn_3-THB	−14.21	NM	0.8
β-Zr_3-THB	−17.44	FM	28.7
β-Cd_3-THB	−10.34	NM	1.1
β-Pb_3Au_4-THB	−3.96	NM	19.1
β-Bi_3Ag_4-THB*	−0.49	NM	6.4
β-Bi_3Au_4-THB*	−1.90	NM	46.7

a) The MOF compositions, formation energy E_F, MGS, and SOC gap E_g^{SOC} are presented at the corresponding high symmetry points (namely, Γ or K). Candidates marked with * are TIs with TFBs sitting on the Fermi level. FM refers to ferromagnetic, and NM refers to nonmagnetic.

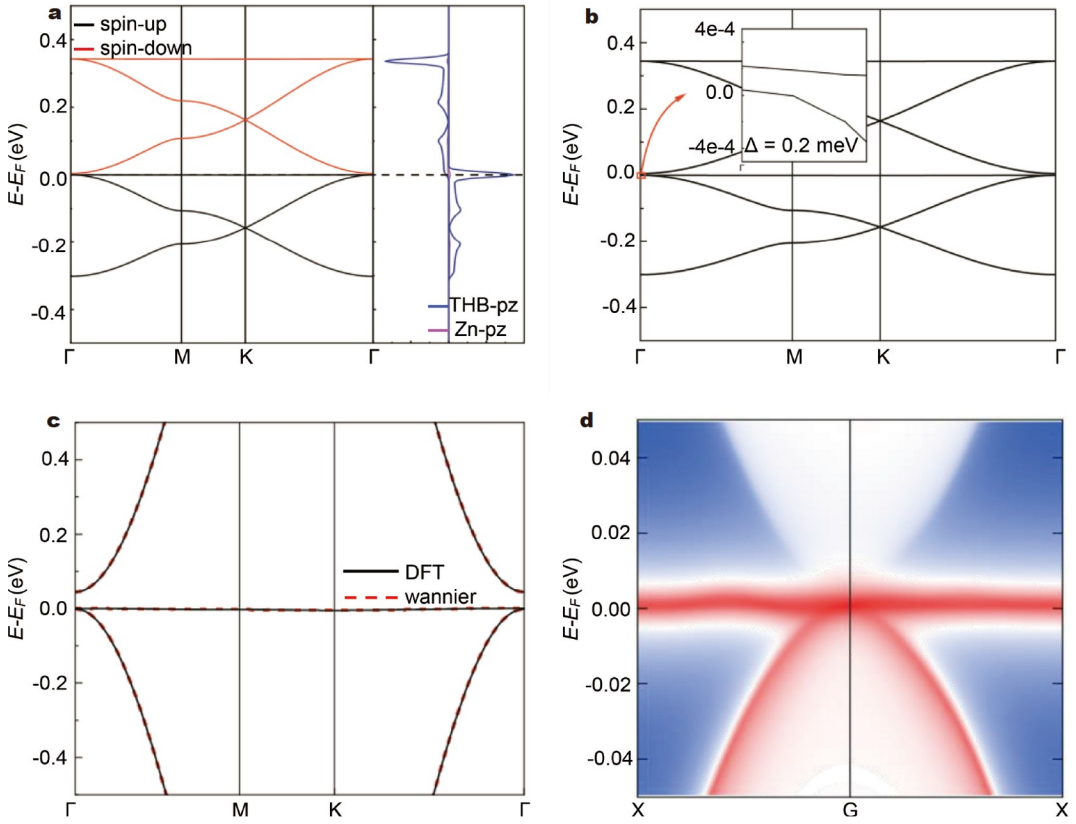

Figure 3 Electronic structures and topological properties of FM state α-Zn_3-THB. (a) DFT-calculated band structures and the projected DOS of α-Zn_3-THB without SOC. (b) Band structures of α-Zn_3-THB with SOC included. (c) Comparison between DFT band structures with SOC and the Wannier band structure near the Fermi level. (d) Semi-infinite edge states of α-Zn_3-THB.

proving the topological nontrivial nature of this structure. Fig. 3d demonstrates the edge state calculated based on the tight banding model using the open-source package Wanniertools [37]. A clear edge state is seen, further proving the topological nontrivial nature of this edge state.

Although α-Zn_3-THB is a typical quantum anomalous Hall insulator with a typical TFB, its nontrivial gap is too narrow to be experimentally observed and confirmed. Therefore, we turn to α-Pb_3Zn_4-THB, which has a considerably larger SOC gap due to the strong SOC effect that Pb atoms induce. Fig. 4 shows the electronic and topological properties of the α-Pb_3Zn_4-THB structure. Its calculated lattice constant is 21.48 Å. Similar to α-Zn_3-THB, α-Pb_3Zn_4-THB has an FM ground state with a magnetic moment of 2 μB per unit cell when the SOC effect is omitted and a total energy that is 70 meV lower than the NM state.

The electronic structure of FM state α-Pb_3Zn_4-THB is shown in Fig. 4a. The magnetic moment mainly comes from Pb atoms in the cluster, in contrast to α-Zn_3-THB. We perform a Bader charge analysis on this system and find each Pb atom loses ~0.6 electrons, each Zn atom loses ~0.5 electrons, and each oxygen atom gains ~1.1 electrons. This result indicates that Pb atoms also participate in the bonding between metal clusters and the ligands. Therefore, we conclude that introducing Pb changes the bonding between the clusters and THB molecules, resulting in a substantially different magnetic distribution. The spin density of α-Pb_3Zn_4-THB is presented in Fig. S2b to provide detailed information on the magnetic state. The PDOS verifies the key role of Pb p_z electrons. For comparison, we provide the band structures and PDOS of the NM state in Fig. 4b. For the FM and NM states, Pb atoms greatly contribute to the bands near the Fermi level, explaining the large SOC gap of this system. To our surprise, α-Pb_3Zn_4-THB has an NM ground state of 103 meV below the FM state when the SOC effect is considered, making it a quantum spin Hall insulator (QSHI). The SOC band structure shown in Fig. 4c matches the NM band structure without SOC pretty well. Calculations considering on-site Coulomb interactions give the same result. The same phase transition is also found in β-Bi_3Cd_4-THB and β-Bi_3Hg_4-THB systems (their band structures are shown in Fig. S3), indicating that this phenomenon is not a mere exception or structure-related property of the α configuration. Notably, this FM-NM transition only appears when the clusters in our calculations comprise heavy elements and IIB elements, for instance, Pb_3Zn_4 and Bi_3Cd_4.

The stability of the FM and NM states can be determined from the exchange splitting E_{ex} and the bandwidth W of the corresponding bands. In this system, E_{ex} refers to the energy difference between spin-up and spin-down bands, and W refers to the bandwidth of the top Dirac band. When $E_{ex} > W$, the FM state is favored; otherwise, the NM state is favored [38]. Because the magnetic moment of α-Pb_3Zn_4-THB mainly comes from Pb atoms, we assume that the strong SOC of Pb is the main cause of this FM-NM transition. For the α-Pb_3Zn_4-THB system, the exchange splitting E_{ex} is larger than W because the bandwidth is split when SOC is omitted. The electrons thus favor filling the spin-up and -down bands separately, resulting in the FM ground state. However, after including SOC, the strong SOC effect of Pb atoms reverses the relation. W slightly changes, but E_{ex}

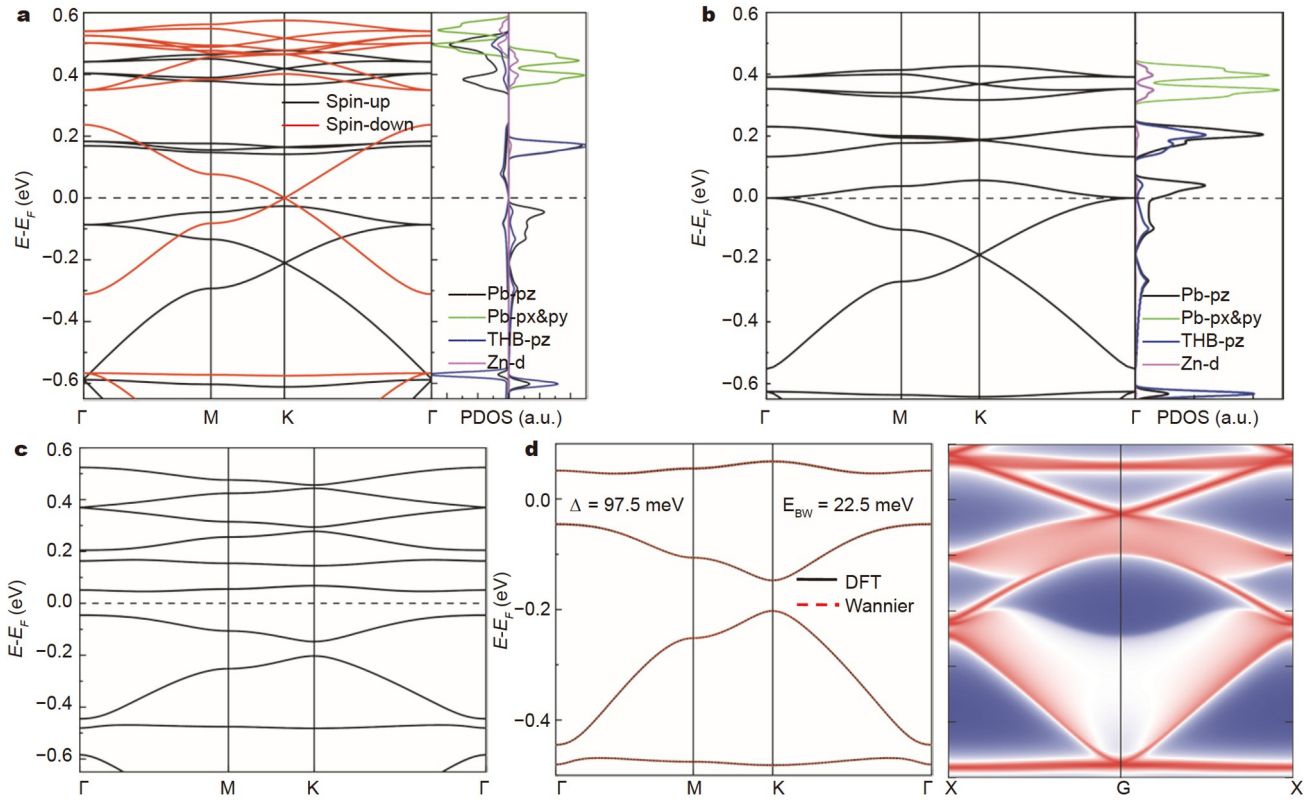

Figure 4 Electronic structures and topological properties of α-Pb_3Zn_4-THB. (a) DFT-calculated band structures and DOS of FM α-Pb_3Zn_4-THB without SOC. (b) Band structures and DOS of NM α-Pb_3Zn_4-THB without SOC. (c) Band structures of α-Pb_3Zn_4-THB with the SOC effect included. (d) Comparison between DFT band structures with SOC and Wannier band structures near the Fermi level and the semi-infinite edge states of α-Pb_3Zn_4-THB within SOC gaps.

substantially decreases. Because the bands near the Fermi level are mainly contributed to by Pb p_z electrons, the SOC of Pb, in particular, results in a considerable change in E_{ex}. Therefore, $E_{ex} < W$ when SOC is involved, leading to an NM-favored ground state. In this particular case, the heavy atoms with strong SOC contribute greatly to the electron occupations of bands near the Fermi level. Thus, SOC can considerably interfere with the band-filling near the Fermi level, eventually causing the FM–NM transition. The β-Bi_3Cd_4 case can be explained similarly. This phase transition is not found in other X_3Y_4-THB-involved candidates such as α-Pb_3Cu_4-THB because the heavy atom contribution to bands near the Fermi level is unsubstantial, which also explains why they do not have large SOC gaps similar to the α-Pb_3Zn_4-THB system.

To verify our hypothesis, we investigate the magnetic states of α-Sn_3Zn_4-THB for comparison by simply replacing Pb with Sn in the α-Pb_3Zn_4-THB lattice. Because Sn has a much weaker SOC effect, such magnetic phase transitions may not occur in the α-Sn_3Zn_4-THB system. Consequently, non-SOC and SOC calculations show an FM ground state (Fig. S4), and the FM-NM transition indeed disappears. These calculation results support our hypothesis above, indicating the key role of SOC effects in the unusual magnetic phase transition.

After identifying the ground state with SOC included, we proceed with a TB model construction using MLWFs to calculate the topological properties, as shown in Fig. 4d. As the system favors the NM state when SOC is considered, we designate α-Pb_3Zn_4-THB as a QSHI with a TFB. Notably, α-Pb_3Zn_4-THB exhibits an SOC gap of 97.5 meV and a flat bandwidth of 22.5 meV, representing a notably large gap in comparison to previously reported QSHIs with TFBs. The right panel of Fig. 4d presents the edge state of α-Pb_3Zn_4-THB based on the TB model. The observed spin nondegenerate edge state between the top flat band and the underlying Dirac band is gapless, confirming α-Pb_3Zn_4-THB as a topological nontrivial system hosting the QSHE. Additionally, we calculate the Z_2 topological invariant within the gap between the flat band and the top Dirac band, and the obtained result $Z_2 = 1$ further corroborates the topological properties of α-Pb_3Zn_4-THB. Interestingly, nontrivial edge states are located approximately 0.45 eV below and 0.10 eV above the Fermi level, situated within the gap between the two Kagome bands. These unexpected edge states may arise from band inversions between different Kagome band sets, potentially influenced by the strong SOC of Pb atoms.

CONCLUSIONS

In this study, we embarked on an investigation of 232 MOF structures composed of metal clusters and THB molecules, drawing inspiration from previous experimental works. Our objective was to identify 2D TIs with enhanced SOC gaps. To this end, we introduced post-transition metal atoms, specifically Tl, Pb, and Bi, into the metal clusters, as they offer stronger SOC effects. Because of this strategic approach, we successfully identified 16 promising 2D-OTIs from the pool of 232 struc-

tures. Our strategy for enhancing the SOC gap is highly practical, as evidenced by the discovery of α-Pb_3Zn_4-THB, an extraordinary system with an SOC gap exceeding 90 meV. This substantial SOC effect even triggers a fascinating FM–NM phase transition. Furthermore, α-Pb_3Zn_4-THB emerges as an intriguing TI characterized by the presence of a TFB. The unique properties of this flat band raise the possibility of hosting various exotic phenomena, such as the FQHE. Our research findings expand the horizon of possibilities for 2D-OTIs and offer a promising avenue for designing 2D topological MOFs with significant topological band gaps, facilitated by the strategic doping of heavy elements. This study paves the way for the exploration of novel materials and devices, holding potential implications for advancing the field of topological materials and quantum phenomena research.

Received 16 November 2023; accepted 1 March 2024; published online 25 March 2024

1 Kane CL, Mele EJ. Quantum spin Hall effect in graphene. Phys Rev Lett, 2005, 95: 226801
2 Bernevig BA, Zhang SC. Quantum spin Hall effect. Phys Rev Lett, 2006, 96: 106802
3 Hasan MZ, Kane CL. *Colloquium*: Topological insulators. Rev Mod Phys, 2010, 82: 3045–3067
4 Knez I, Du RR, Sullivan G. Evidence for helical edge modes in inverted InAsGaSb quantum wells. Phys Rev Lett, 2011, 107: 136603
5 Qi XL, Zhang SC. Topological insulators and superconductors. Rev Mod Phys, 2011, 83: 1057–1110
6 Liu J, Hsieh TH, Wei P, *et al.* Spin-filtered edge states with an electrically tunable gap in a two-dimensional topological crystalline insulator. Nat Mater, 2014, 13: 178–183
7 Zhou M, Ming W, Liu Z, *et al.* Epitaxial growth of large-gap quantum spin Hall insulator on semiconductor surface. Proc Natl Acad Sci USA, 2014, 111: 14378–14381
8 Gao L, Sun JT, Sethi G, *et al.* Orbital design of topological insulators from two-dimensional semiconductors. Nanoscale, 2019, 11: 22743–22747
9 Jin KH, Jiang W, Sethi G, *et al.* Topological quantum devices: A review. Nanoscale, 2023, 15: 12787–12817
10 Liu F. Two-dimensional topological insulators: Past, present and future. Coshare Sci, 2023, 1: 1–62
11 Liu Z, Wang ZF, Mei JW, *et al.* Flat chern band in a two-dimensional organometallic framework. Phys Rev Lett, 2013, 110: 106804
12 Wang ZF, Liu Z, Liu F. Organic topological insulators in organometallic lattices. Nat Commun, 2013, 4: 1471
13 Wang ZF, Liu Z, Liu F. Quantum anomalous Hall effect in 2D organic topological insulators. Phys Rev Lett, 2013, 110: 196801
14 Zhang X, Zhao M. Robust half-metallicity and topological aspects in two-dimensional Cu-TPyB. Sci Rep, 2015, 5: 14098
15 Sun H, Li B, Zhao J. Half-metallicity in 2D organometallic honeycomb frameworks. J Phys-Condens Matter, 2016, 28: 425301
16 Yamada MG, Soejima T, Tsuji N, *et al.* First-principles design of a half-filled flat band of the kagome lattice in two-dimensional metal-organic frameworks. Phys Rev B, 2016, 94: 081102
17 Chen Y, Sun Q. Magnetic two-dimensional organic topological insulator: Au–1,3,5-triethynylbenzene framework. J Chem Phys, 2017, 147: 104704
18 Zhang LZ, Wang ZF, Huang B, *et al.* Intrinsic two-dimensional organic topological insulators in metal–dicyanoanthracene lattices. Nano Lett, 2016, 16: 2072–2075
19 Sun H, Tan S, Feng M, *et al.* Deconstruction of the electronic properties of a topological insulator with a two-dimensional noble metal–organic honeycomb–Kagome band structure. J Phys Chem C, 2018, 122: 18659–18668
20 Gao Y, Zhang YY, Sun JT, *et al.* Quantum anomalous Hall effect in two-dimensional Cu-dicyanobenzene coloring-triangle lattice. Nano Res, 2020, 13: 1571–1575
21 Jiang W, Ni X, Liu F. Exotic topological bands and quantum states in metal–organic and covalent–organic frameworks. Acc Chem Res, 2021, 54: 416–426
22 Jiang W, Huang H, Liu F. A Lieb-like lattice in a covalent-organic framework and its Stoner ferromagnetism. Nat Commun, 2019, 10: 2207
23 Zhang J, Shchyrba A, Nowakowska S, *et al.* Probing the spatial and momentum distribution of confined surface states in a metal coordination network. Chem Commun, 2014, 50: 12289–12292
24 Yan L, Pohjavirta I, Alldritt B, *et al.* On-surface assembly of Au-dicyanoanthracene coordination structures on Au(111). ChemPhysChem, 2019, 20: 2297–2300
25 Hernández-López L, Piquero-Zulaica I, Downing CA, *et al.* Searching for kagome multi-bands and edge states in a predicted organic topological insulator. Nanoscale, 2021, 13: 5216–5223
26 Yan L, Silveira OJ, Alldritt B, *et al.* Synthesis and local probe gating of a monolayer metal-organic framework. Adv Funct Mater, 2021, 31: 2100519
27 Kambe T, Sakamoto R, Hoshiko K, *et al.* π-conjugated nickel bis(dithiolene) complex nanosheet. J Am Chem Soc, 2013, 135: 2462–2465
28 Wang ZF, Su N, Liu F. Prediction of a two-dimensional organic topological insulator. Nano Lett, 2013, 13: 2842–2845
29 Bebensee F, Svane K, Bombis C, *et al.* A surface coordination network based on copper adatom trimers. Angew Chem Int Ed, 2014, 53: 12955–12959
30 Yan L, Xia B, Zhang Q, *et al.* Stabilizing and organizing Bi_3Cu_4 and Bi_7Cu_{12} nanoclusters in two-dimensional metal–organic networks. Angew Chem Int Ed, 2018, 57: 4617–4621
31 Kresse G, Furthmüller J. Efficient iterative schemes for *ab initio* total-energy calculations using a plane-wave basis set. Phys Rev B, 1996, 54: 11169–11186
32 Perdew JP, Burke K, Ernzerhof M. Generalized gradient approximation made simple. Phys Rev Lett, 1996, 77: 3865–3868
33 Bocquet AE, Mizokawa T, Saitoh T, *et al.* Electronic structure of 3d-transition-metal compounds by analysis of the 2p core-level photoemission spectra. Phys Rev B, 1992, 46: 3771–3784
34 Dudarev SL, Botton GA, Savrasov SY, *et al.* Electron-energy-loss spectra and the structural stability of nickel oxide: An LSDA + *U* study. Phys Rev B, 1998, 57: 1505–1509
35 Tang E, Mei JW, Wen XG. High-temperature fractional quantum Hall states. Phys Rev Lett, 2011, 106: 236802
36 Mostofi AA, Yates JR, Lee YS, *et al.* Wannier90: A tool for obtaining maximally-localised Wannier functions. Comput Phys Commun, 2008, 178: 685–699
37 Wu QS, Zhang SN, Song HF, *et al.* WannierTools: An open-source software package for novel topological materials. Comput Phys Commun, 2018, 224: 405–416
38 Zhang L, Park C, Yoon M. Quantum phase engineering of two-dimensional post-transition metals by substrates: Toward a room-temperature quantum anomalous Hall insulator. Nano Lett, 2020, 20: 7186–7192

Acknowledgements This work was supported by the National Key R&D Program of China (2019YFA0308500 and 2022YFA1204103), the National Natural Science Foundation of China (52250402, 52201231, 22372047, and 61888102), the Chinese Academy of Sciences (CAS) Project for Young Scientists in Basic Research (YSBR-003), and the Fundamental Research Funds for the Central Universities. A portion of the research was performed in the CAS Key Laboratory of Vacuum Physics.

Author contributions Yin Y performed the high-throughput calculations, data processing, and original drafting. Gao Y, Zhang L, Zhang YY, and Du S carried out the supervision, draft reviewing and editing. Zhang L and Zhang YY conceived and supervised the research. Zhang L and Zhang YY directed the manuscript writing and revision. All the authors assisted in writing and revising the manuscript. All authors read and approved the final manuscript.

Conflict of interest The authors declare that they have no conflict of interest.

Supplementary information Supporting data are available in the online version of the paper.

Yiyang Yin is a PhD student at the School of Physical Sciences, University of Chinese Academy of Sciences, under the supervision of Prof. Yu-Yang Zhang. His research interest mainly focuses on the theoretical study of 2D organic topological insulators.

Yu-Yang Zhang obtained his PhD degree from the Institute of Physics, the Chinese Academy of Sciences in 2011. He then worked as a postdoctoral fellow at Rensselaer Polytechnic Institute and Vanderbilt University in the United States. Since 2016, he has been an associate professor at the University of Chinese Academy of Sciences. His recent research interest lies in designing low-dimensional materials with novel properties.

Y_3-/X_3Y_4-THB金属有机网络中本征二维拓扑绝缘体的预测

殷翼扬[1], 高艺璇[1], 张礼智[2], 张余洋[1*], 杜世萱[1]

摘要 本工作利用基于密度泛函理论的高通量计算方法，研究了由金属团簇和四羟基苯(THB)分子形成的232个具有Kagome晶格的有机金属网格. 在由THB分子和过渡金属原子三聚体(称为Y_3-THB)组成的有机金属网格中，有7种网格结构是本征有机拓扑绝缘体. 进一步引入过渡金属原子(Tl, Pb, Bi)后得到的X_3Y_4-THB结构中, 发现了9个具有较大自旋轨道耦合能隙的本征有机拓扑绝缘体. 在这些本征拓扑绝缘体中, α相Pb_3Zn_4-THB结构是具有拓扑平带的拓扑绝缘体，其非平庸自旋轨道耦合能隙(97.5 meV)几乎是其平带带宽(22.5 meV)的4倍，是实现分数量子霍尔效应的理想平台. 该工作为设计具有大能隙的二维有机拓扑绝缘体提供了新的途径.